Finite-size scaling of eigenstate thermalization

W. Beugeling, R. Moessner, and Masudul Haque
Max-Planck-Institut für Physik komplexer Systeme, Nöthnitzer Straße 38, 01187 Dresden, Germany
(Received 29 August 2013; revised manuscript received 14 November 2013; published 4 April 2014)

According to the eigenstate thermalization hypothesis (ETH), even isolated quantum systems can thermalize because the eigenstate-to-eigenstate fluctuations of typical observables vanish in the limit of large systems. Of course, isolated systems are by nature finite and the main way of computing such quantities is through numerical evaluation for finite-size systems. Therefore, the finite-size scaling of the fluctuations of eigenstate expectation values is a central aspect of the ETH. In this work, we present numerical evidence that for generic nonintegrable systems these fluctuations scale with a universal power law $D^{-1/2}$ with the dimension D of the Hilbert space. We provide heuristic arguments, in the same spirit as the ETH, to explain this universal result. Our results are based on the analysis of three families of models and several observables for each model. Each family includes integrable members and we show how the system size where the universal power law becomes visible is affected by the proximity to integrability.

DOI: 10.1103/PhysRevE.89.042112 PACS number(s): 05.30.−d, 05.70.Ln, 75.10.Pq

I. INTRODUCTION

In recent years, nonequilibrium unitary evolution of isolated quantum systems has emerged as a key topic in many-body physics. In this context, the issue of thermalization in isolated quantum systems has received fresh and growing attention. The eigenstate thermalization hypothesis (ETH) is widely thought to encapsulate the mechanism by which thermalization occurs in isolated nonintegrable systems [1–3].

The basic statement of the ETH is that, for a large isolated system, the diagonal matrix elements of typical observables in the Hamiltonian eigenstate basis, known as the eigenstate expectation values (EEVs), depend smoothly on the corresponding energy eigenvalues. Despite intense recent research [3–20], the understanding of several aspects of the ETH remains incomplete. For example, it is not fully known exactly which observables will or will not serve as typical observables. Another issue is the specification of large isolated systems: How large does the system have to be? Clearly, a proper understanding of this question requires a finite-size scaling study of the ETH. This is an important question for any actual experimental study of thermalization because any isolated system is in practice finite. Size dependence is also vital for evaluating numerical studies, which are performed on finite systems. This is the subject of the present paper.

It is generally understood that the fluctuations $\sigma_{\Delta A}$ of EEVs should decrease exponentially with system size [1,8,10,20] so that the EEVs become very smooth as a function of energy for reasonably large isolated systems. For discrete systems with a finite Hilbert space, this means a power-law dependence of the fluctuations with the dimension D of the Hilbert space. In this work, we identify the exponent of this power-law behavior as $-\frac{1}{2}$. Examining several nonintegrable models, we provide strong numerical evidence for $\sim D^{-1/2}$ behavior of EEV fluctuations. The $D^{-1/2}$ behavior generally becomes clear only at the largest sizes accessible through full numerical diagonalization. Our analysis therefore uses a comparison of several sizes, at varying distances from integrability. We use Hamiltonians designed to be tunable between two integrable limits and thus examine how this finite-size dependence is affected by proximity to integrable points. As the integrable points are approached, larger sizes are required for the $D^{-1/2}$ behavior to set in and for purely integrable systems the size dependence is no longer $D^{-1/2}$.

The exponent $-\frac{1}{2}$ suggests the central limit theorem, which would predict power-law dependences if $\sigma_{\Delta A}$ is the average of $O(D)$ random variables. We distinguish between two plausible mechanisms and identify the correct explanation: The exponent arises from the averaging over effectively random coefficients of individual eigenstates and not from an average over $O(D)$ eigenstates in the definition of $\sigma_{\Delta A}$. This explanation relies on assumptions of effective randomness, which are difficult to prove rigorously but are in the same spirit as the ETH itself. A particularly nontrivial aspect is that it is not immediately obvious why this argument should break down for integrable systems. While the concept of effective randomness provides useful insight, the unavoidably heuristic nature of such arguments means that our numerical analysis is essential for determining the finite-size scaling of EEV fluctuations.

We use several observables for each model Hamiltonian to show the validity of the $D^{-1/2}$ law for a wide variety of observables. Unlike some of the previous studies of the ETH (e.g., [3]), we do not refer to particular quench protocols, which corresponds loosely to focusing on particular parts of the eigenspectrum. Instead, we examine the complete spectrum and thus a broad class of quantum quenches. The robustness of our results for different observables, Hamiltonians, and quench protocols provides compelling evidence for the universality of the $D^{-1/2}$ scaling.

The structure of this article is as follows. In Sec. II we introduce our measure for the amplitude of EEV fluctuations. We define our models and observables in Sec. III. The $D^{-1/2}$ scaling of the EEV fluctuations is presented in Sec. IV, where we give both numerical results and a heuristic argument. The conclusion and discussion are in Sec. V. The Appendixes provide further details: Appendix A discusses issues related to our definition of the EEV fluctuations, Appendix B elaborates on the heuristic argument for $D^{-1/2}$ scaling, and Appendix C provides detail on the numerical methods.

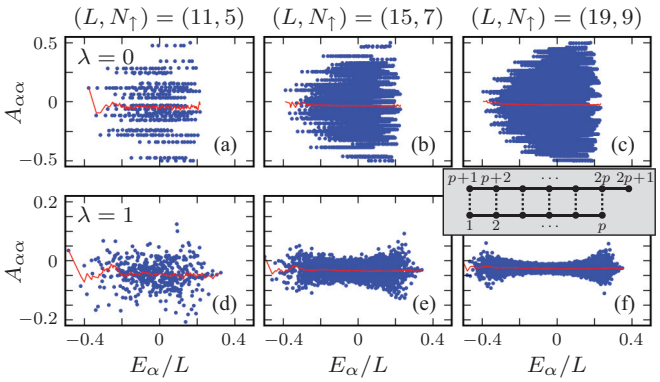

FIG. 1. (Color online) Eigenstate expectation values (blue dots) and the microcanonical average (red curves) for the observable $\hat{A} = S_2^z$ with (a)–(c) $\lambda = 0$ and (d)–(f) $\lambda = 1$ for three different system sizes L. The energies on the horizontal axis are scaled by system size for meaningful comparison. [The microcanonical average is nearly constant in this case, which is not representative for all observables (see e.g., Refs. [6,14]).] The inset shows the geometry of the ladder system and site labeling. Solid and dashed lines are H_{leg} and H_{rung} couplings, respectively.

II. FORMULATION: EEV FLUCTUATIONS

The ETH states that the diagonal matrix element of a typical operator $\hat{A}$ in the eigenstates $|\psi_\alpha\rangle$ of the Hamiltonian, i.e., the EEVs $A_{\alpha\alpha} = \langle\psi_\alpha|\hat{A}|\psi_\alpha\rangle$, vary smoothly with the corresponding energy eigenvalues E_α. Thus, the EEVs may be considered as constant within an energy window $[E - \Delta E, E + \Delta E]$. In other words, the values of $A_{\alpha\alpha}$ approximately coincide with the microcanonical average $\langle\hat{A}\rangle_\mu(E_\alpha, \Delta E)$, defined as the average EEV within this window:

$$\langle\hat{A}\rangle_\mu(E, \Delta E) = \frac{1}{N_{E,\Delta E}} \sum_{\alpha: E_\alpha \in [E-\Delta E, E+\Delta E]} A_{\alpha\alpha}, \qquad (1)$$

where $N_{E,\Delta E}$ is the number of states in this window. If the initial nonequilibrium state has weights constrained to such a microcanonical window, then the ETH guarantees that the long-time average will be equal to the canonical expectation value.

We wish to study how this behavior is approached with increasing system size. Therefore, we study the fluctuations around the microcanonical average as a function of size. For every α we define $\Delta A_\alpha = A_{\alpha\alpha} - \langle A\rangle_\mu(E_\alpha, \Delta E)$. We then consider the statistical properties of ΔA_α over a large part of the Hilbert space. In the following, we take averages over all states in the central 20% of the total energy range of the spectrum, which we denote by $\langle\cdots\rangle_c$. This average typically includes more than half of all eigenstates. The highest and lowest ends of the spectrum are left out because the spectrum edges are likely to show atypical behavior (see Fig. 1). The EEV fluctuations $\sigma_{\Delta A}$ are defined as the standard deviation of ΔA,

$$\sigma^2_{\Delta A}(\Delta E) \equiv \langle[\Delta A_\alpha]^2\rangle_c \equiv \langle[A_{\alpha\alpha} - \langle A\rangle_\mu(E_\alpha, \Delta E)]^2\rangle_c. \quad (2)$$

We note that $\sigma_{\Delta A}$ cannot be interpreted as a standard deviation of the $A_{\alpha\alpha}$ because of the microcanonical average $\langle\cdots\rangle_\mu$ rather than the ordinary average $\langle\cdots\rangle$ on the right-hand side of Eq. (2). In the definition above we have assumed that the average of ΔA is negligible, i.e., that

$$\text{var}(\Delta A_\alpha) \equiv \langle\Delta A_\alpha^2\rangle_c - \langle\Delta A_\alpha\rangle_c^2 \approx \langle\Delta A_\alpha^2\rangle_c. \qquad (3)$$

While the smallness of ΔA_α is intuitively reasonable, the definition of ΔA_α in terms of the microcanonical average does not guarantee *a priori* that

$$\langle\Delta A_\alpha\rangle_c^2 \ll \langle\Delta A_\alpha^2\rangle_c \qquad (4)$$

is valid. Numerical evidence for the validity of this inequality is presented in Appendix A. Given that this condition holds, the interpretation of $\sigma_{\Delta A}$ defined in Eq. (2) as a standard deviation of ΔA is justified.

In Fig. 1 the energies are divided by the system size L. The reason is that the upper and lower parts of the energy spectrum scale as L, thus the spectrum appears in the same range of E_α/L. The microcanonical average curves for the EEVs also look roughly similar for different sizes, when plotted against E_α/L, as does the density of states.

The dependence of $\sigma_{\Delta A}$ on the width ΔE of the microcanonical window is weak as long as the range $[E - \Delta E, E + \Delta E]$ contains sufficiently many states for good statistics while it remains sufficiently narrow so that the microcanonical average follows the EEVs well. As a good tradeoff for satisfying both these conditions, we have used the value $\Delta E = 0.025L$ for all following results. Justification for this value can be found in Appendix A. As with the horizontal axes in Fig. 1, we rescale the window width by keeping $\Delta E/L$ constant. This window thus contains approximately equal fractions of the total number of eigenstates for different values of L.

III. MODELS AND OBSERVABLES

A. Tunable model Hamiltonians

We will present results for three families of Hamiltonians. These are designed to be tunable toward or away from integrable limits, to have good thermodynamic limits, and to avoid symmetries that lead to degeneracies in the spectrum. We use systems with a Hamiltonian of the form $H = H_0 + \lambda H_1$ such that the model is integrable if the control parameter λ is 0 or ∞. For $\lambda \in (0, \infty)$, the system is nonintegrable.

The first two are based on the spin-$\frac{1}{2}$ anisotropic Heisenberg (XXZ) chain, which is integrable via the Bethe ansatz [21]. These Hamiltonians commute with the total z component of spin, so the number $N_\uparrow$ of up spins is conserved. We examine finite-size scaling by increasing $(L, N_\uparrow)$. To suppress unwanted symmetries, e.g., SU(2), we take the anisotropy Δ to be away from 0 or 1; results are presented for $\Delta = 0.8$.

The Heisenberg ladder consists of two coupled XXZ chains (see Fig. 1, inset). The Hamiltonian for the $L = (2p + 1)$-site model is given by $H_{\text{ladder}} = H_{\text{leg}} + \lambda H_{\text{rung}}$, where

$$H_{\text{leg}} = \sum_{i=1}^{p-1} h_{i,i+1} + \sum_{i=p+1}^{2p} h_{i,i+1}, \quad H_{\text{rung}} = \sum_{i=1}^{p} h_{i,i+p} \qquad (5)$$

are the intrachain and interchain (rung) couplings, respectively, given in terms of the Heisenberg XXZ coupling

$$h_{i,j} \equiv \tfrac{1}{2}(S_i^+ S_j^- + S_i^- S_j^+) + \Delta S_i^z S_j^z, \qquad (6)$$

where $S_i^{\pm} = S_i^x \pm S_i^y$ and S_i^z are the spin operators on site i ($\hbar \equiv 1$). In order to suppress reflection symmetries, one leg has an extra site compared to the other. We will focus on the $S^z_{\rm total}$ sector $N_\uparrow = p$.

The second Hamiltonian is the XXZ chain in a harmonic magnetic trap $H_{\rm trap} = H_{XXZ} + \lambda H_{\rm magn}$, with the open-$XXZ$-chain and magnetic-field terms

$$H_{XXZ} = \sum_{i=1}^{L-1} h_{i,i+1}, \quad H_{\rm magn} \equiv -\sum_{i=1}^{L} B_i S_i^z, \tag{7}$$

respectively. Here λB_i denotes the magnetic field at site i where λ parametrizes the strength of the trap and $B_i = [2/(L-1)^2][i - i_0]^2$. Here the trap center is near the midpoint of the chain $i_0 = \frac{1}{2}(L+1) - \Delta i$, with a shift Δi that we choose to be irrational to avoid symmetries. The factor $2/(L-1)^2$ ensures a meaningful thermodynamic limit. We use the sector of filling factor $\frac{1}{3}$ by defining $L = 3N_\uparrow$. A harmonic trap is a particularly important manner of breaking integrability since the classic experiment exploring the role of integrability in time evolution [22] involved dynamics in a harmonic trap.

The third Hamiltonian is the Bose-Hubbard model on an open chain

$$H_{\rm BH} = -\sum_{i=1}^{L-1}(b_i^\dagger b_{i+1} + b_{i+1}^\dagger b_i) + \lambda \sum_{i=1}^{L} b_i^\dagger b_i^\dagger b_i b_i, \tag{8}$$

where $b_i^\dagger$ and b_i are the bosonic creation and annihilation operators at sites i [23]. The model is integrable when only kinetic or only interaction terms are present, i.e., in the $\lambda = 0$ and $\lambda \to \infty$ limits. We avoid reflection symmetry by modifying the interaction at site 1 to be 1.1λ instead of λ. We present results for half filling, i.e., the number of bosons is $N_{\rm b} = \frac{1}{2}L$.

B. Observables

An important issue in ETH studies is the question of which observables the ETH applies to. To show that our main result ($\sigma_{\Delta A} \sim D^{-1/2}$ behavior) is valid for a wide range of observables, we use a number of different one-site and two-site observables. For the ladder model, we use the spin z component S_i^z at site i and sums of these quantities with i running over multiple sites, e.g., all sites of the bottom leg $S^z_{\rm bottom}$. We also consider the two-site operators $C^z_{i,j} \equiv S_i^z S_j^z$ and sums of such operators over regions of the system. We similarly study a set of one- and two-site operators and their sums over regions of the system for the XXZ chain in a trap and for the Bose-Hubbard model: For the XXZ chain, we consider one-site (e.g., S_i^z) and two-site spin operators (e.g., $C^z_{i,j} = S_i^z S_j^z$ and $C^{xy}_{i,j} \equiv S_i^+ S_j^- + S_i^- S_j^+$) and their sums over the middle one-third sites ($S^z_{\rm middle}$, $C^z_{\rm middle}$, and $C^{xy}_{\rm middle}$). For the Bose-Hubbard model, we use on-site occupancies $n_i = b_i^\dagger b_i$, occupancies summed over the central sites [$n_{\rm middle} = \sum_{i=i'+1}^{L-i'} n_i/(L-2i')$ with $i' = \lfloor (L+2)/4 \rfloor$], and the operators for nearest-neighbor two-point and four-point correlators ($b_i^\dagger b_{i+1} + b_{i+1}^\dagger b_i$ and $n_i n_{i+1}$).

IV. SCALING ANALYSIS OF EEV FLUCTUATIONS

A. Dependence on size and integrability

Figures 1 and 2 provide visual displays of some of the more dramatic aspects of the ETH. In Fig. 1 we use as observable S_2^z, the z component of the spin at site $i = 2$. At the integrable point, the width of the distribution of EEVs can be seen to stay unchanged with system size [Figs. 1(a)–1(c)]. For the nonintegrable model, the EEV fluctuations clearly decrease with system size in the bulk of the spectrum. The top and the bottom of the spectrum do not show a similarly dramatic decrease with system size, demonstrating that the ETH should be considered relevant primarily to the bulk of the spectrum. The physical reason is that the edges of the spectrum tend to show emergent integrable (e.g., Luttinger liquid) behavior.

Figure 2 shows the typical dependence of EEV fluctuations on the parameter λ for different system sizes. This plot corroborates the intuition that for increasing system size the fluctuations decay faster away from the integrable limits than close to them. For larger systems there is a pronounced minimum of $\sigma_{\Delta A}$ at intermediate λ, where it is farthest from both integrable limits.

For the observable $\hat{A} = S^z_{\rm bottom}$ in the ladder system [Fig. 2(b)], $\sigma_{\Delta A}$ is smaller in the $\lambda \sim 1$ regime than it is in the integrable regions, even for the smallest system sizes. For the observable $\hat{A} = C^z_{2,p+2} = S_2^z S^z_{p+2}$ [Fig. 2(a)], some deviation is seen for very small systems, but the characteristic behavior sets in already at moderate sizes. This overall qualitative behavior is very typical and is similar for all observables and all models we have investigated. The system size at which the crossover to large-system behavior (pronounced minimum in the nonintegrable regime) takes place depends on the model and on the observable.

B. Scaling with system size

In Figs. 3(a)–3(c) we show the dependence of the EEV fluctuations on Hilbert-space size D for several values of the rung coupling parameter λ that tunes the system away from integrability. The data plotted in this figure involve vertical slices of the plots in Fig. 2 (size dependence at constant λ values). The ETH fluctuations are commonly claimed to decrease exponentially with system size for nonintegrable models and hence should decrease as a power law with D. We define an exponent e as the one that is obtained in a power-law

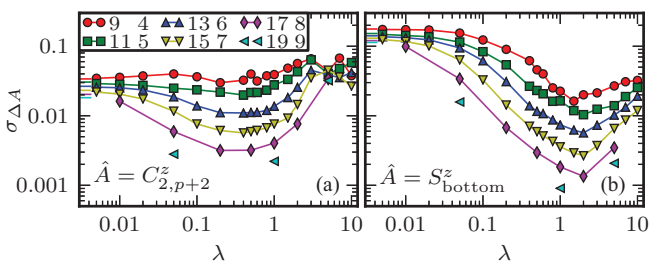

FIG. 2. (Color online) Fluctuation amplitudes $\sigma_{\Delta A}$ as a function of the control parameter λ. The $\sigma_{\Delta A}$ are presented for the Heisenberg XXZ ladder system for several system sizes $(L, N_\uparrow)$ (see legend) and two different observables [in (a) and (b), respectively].

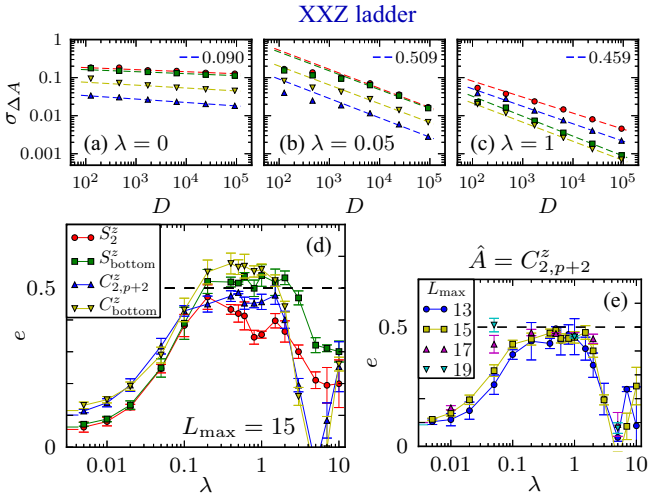

FIG. 3. (Color online) (a)–(c) Dependence of $\sigma_{\Delta A}$ on the Hilbert-space dimension D in the Heisenberg ladder. The different operators $\hat{A}$ used are indicated in the legend for (d). The lines are best fits to $c_0 D^{-e}$; the exponent estimator e is indicated for the operator $C^z_{2,p+2}$. (d) The exponent estimator e is plotted against λ for the four operators. (e) Sizes up to L_{max} are used for fitting to obtain the estimator e. The trend is that $e \to \frac{1}{2}$ for increasing L_{max}.

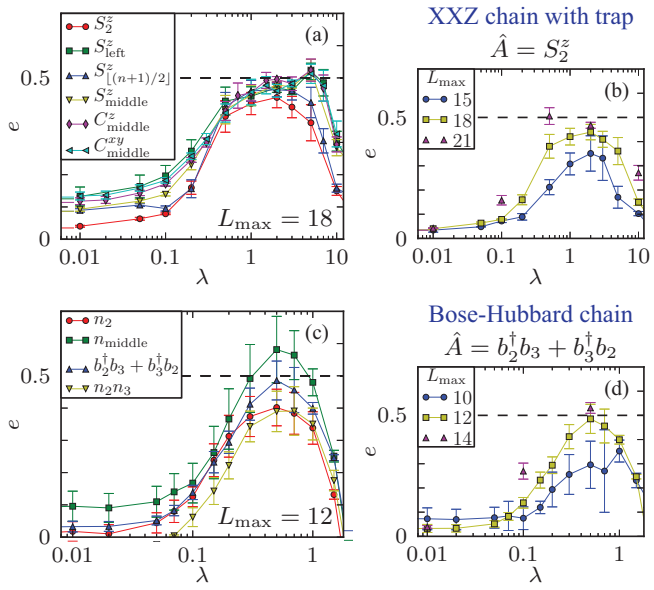

FIG. 4. (Color online) For the XXZ chain in a trap, we plot (a) the exponent estimator e against integrability-breaking parameter λ. The estimator e is calculated with data up to $L_{max} = 18$. The estimator e is calculated with data up to L_{max} sites. (b) Plot of the estimator e obtained from fits with increasing L_{max}. Analogous results for the Bose Hubbard chain are shown in (c) (with $L_{max} = 12$) and (d).

fit $\sim D^{-e}$ to the data for $\sigma_{\Delta A}$ for the available sizes. We make no *a priori* claims about the dependence being actually a power law or the obtained values of e being the actual exponent in the large-size limit. In cases where the dependence is a power law, as expected in nonintegrable systems, e is an estimator for the actual exponent. The exponent estimator e goes toward zero as one approaches the integrable points $\lambda = 0$ or $\lambda = \infty$. At the point $\lambda = 0$ the dependence on D is presumably not even a power law.

Values of the exponent estimator e are plotted in Figs. 3(d) and 3(e) for the ladder system and in Fig. 4 for the XXZ-trap system and the Bose-Hubbard system. There is a clear and general trend for e to cluster around or approach 0.5 in all systems, when away from integrability. Taken together, we believe this provides compelling evidence of a $\sigma_{\Delta A} \sim D^{-1/2}$ dependence in generic nonintegrable systems for generic few-body observables $\hat{A}$. Figure 3(d) displays the general behavior for several different observables in the XXZ ladder: $e \approx \frac{1}{2}$ for intermediate λ and vanishing e for λ approaching 0 or ∞. Similar behavior is observed for the XXZ chain with a trap and for the Bose-Hubbard chain [see Figs. 4(a) and 4(c), respectively]. For the three systems considered here, the results are qualitatively similar. The general trend is that for a fixed maximum system size L_{max}, the exponent estimator e clusters around $\frac{1}{2}$ for intermediate values of λ and has lower values close to the integrable limits. In Figs. 3(e), 4(b), and 4(d) we show more quantitative scaling behavior for the three tunable Hamiltonians by plotting the exponent estimators e derived from power-law fits to the data of system sizes up to L_{max}. We note a crossover from integrablelike to $\sim D^{-1/2}$ behavior for nonintegrable systems close to integrability (e.g., for the XXZ ladder at $\lambda = 0.05$ [see Figs. 3(b) and 3(e)]) as the system size is increased. The trend with increasing L_{max} points to the large-system behavior of $\sigma_{\Delta A}$ being $\sim D^{-1/2}$ over the full range $\lambda \in (0, \infty)$.

C. The $D^{-1/2}$ behavior from eigenstate size: A heuristic argument

The $D^{-1/2}$ dependence of $\sigma_{\Delta A}$ can be argued heuristically by considering projections of eigenstates onto the eigenbasis of the $\hat{A}$ operator and then invoking the central limit theorem. If $\{a_\gamma\}$ and $\{|\phi_\gamma\rangle\}$ denote the eigenvalues and eigenvectors of $\hat{A}$ and we expand the eigenvectors $|\psi_\alpha\rangle$ of H as

$$|\psi_\alpha\rangle = \sum_\gamma c^{(\alpha)}_\gamma |\phi_\gamma\rangle, \tag{9}$$

then we can write the EEVs as

$$A_{\alpha\alpha} = \sum_{\gamma=1}^{D} \left|c^{(\alpha)}_\gamma\right|^2 a_\gamma. \tag{10}$$

This is an average of $X_\gamma \equiv D|c^{(\alpha)}_\gamma|^2 a_\gamma$. Under the hypothesis that the X_γ can be regarded as random variables with D-independent variance, the central limit theorem guarantees that the fluctuations of $A_{\alpha\alpha}$ decrease as $D^{-1/2}$. (This argument is detailed further in Appendix B.) We are unable to *prove* the idea that the X_γ or c_γ act as random variables. However, one can intuitively think of an eigenstate of a nonintegrable system as being so complex that its projections onto the eigenbasis of a typical observable are effectively random. This is similar in spirit to the ETH itself (also difficult to prove rigorously), for which the argument is that when eigenfunctions are complex enough, EEVs of typical observables will contain no signature of the detailed structure of the wave function.

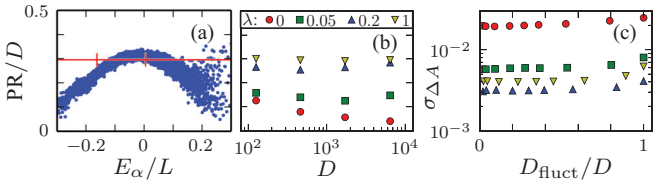

FIG. 5. (Color online) (a) Scaled participation ratios of all eigenstates with respect to the computational basis for 15-site ladder, with $\lambda = 1$. The averaging region is shown by vertical bars and the average PR value is shown by the horizontal line. (b) Dependence of the scaled average PR on D. (c) Dependence of $\sigma_{\Delta A}$ on the number $D_{\rm fluct}$ of states used as input to compute this quantity. Data are for the 17-site ladder with $\hat{A} = C^z_{2,p+2}$ for four different values of λ [shown in the legend in (b)].

This argument relies on the assumption that the size (number of components) of the individual eigenfunctions is $O(D)$. This is justified in Figs. 5(a) and 5(b) through the participation ratio (PR) in the computational (site) basis, defined for each eigenstate as

$$P_\alpha = \left[\sum_\gamma \left| c_\gamma^{(\alpha)} \right|^4 \right]^{-1}. \tag{11}$$

The PR measures the number of basis states contributing to the eigenstate. (For a single state, the commonly discussed inverse participation ratio is $1/P_\alpha$.) Figure 5(b) shows that it is, on average, indeed proportional to D in nonintegrable cases. The $D^{-1/2}$ scaling of $\sigma_{\Delta A}$ and the D scaling of the average PR are, taken together, consistent with the expectation [17] that $\sigma^2_{\Delta A}$ should be proportional to the average inverse PR. The observations of Ref. [17], in terms of the average inverse PR in the momentum Fock basis, can also be cast as a heuristic argument for $D^{-1/2}$ scaling, roughly equivalent to the reasoning above.

We emphasize that the number $D_{\rm fluct}$ of states included in the average $\langle \cdots \rangle_{\rm c}$ does not account for the $D^{-1/2}$ dependence. The quantity $\sigma_{\Delta A}$ is the standard deviation of the distribution of the ΔA_α and it is independent of how many times one probes this distribution, i.e., the number of states that is used to compute $\sigma_{\Delta A}$. As shown in Fig. 5(c), the value of $\sigma_{\Delta A}$ is independent of $D_{\rm fluct}$ as long as states at the edges of the spectrum are avoided. The slight dependence on $D_{\rm fluct}$ is caused by the fact that at the edges of the spectrum, the fluctuations of $A_{\alpha\alpha}$ are different from those in the center of the spectrum. The edges of the spectrum, of course, are outside the purview of the ETH. This demonstrates that the $D^{-1/2}$ behavior arises not from the number of eigenstates averaged over, but from the complexity of the individual eigenstates themselves.

The fluctuations decrease more slowly with system size at the integrable points, as evidenced by the vanishing of the exponent estimator e in the $\lambda \to 0$ and ∞ limits in each of the models. This implies a difference in the structure of the individual eigenstates. One characterization of this difference is visible in Fig. 5(b), where the scaled average PR for the integrable model is seen to decrease with system size. A detailed study of eigenstates in integrable models from this perspective, to complement the studies of Refs. [18–20,24–28], is interesting, but is beyond the scope of the present work.

V. SUMMARY AND DISCUSSION

For nonintegrable systems, we have presented the size dependence of the deviation from the ETH, as measured by the EEV fluctuations, $\sigma_{\Delta A}$, for lattice systems. It is well accepted that $\sigma_{\Delta A}$ decreases exponentially with the system size $\sigma_{\Delta A} \sim \exp[-c_1 L]$, e.g., Ref. [20] has numerical data showing the exponential decay. In terms of the Hilbert-space size D, if $D \sim \alpha^L$ (see Appendix C 2), then

$$\sigma_{\Delta A} \sim D^{-e} \sim \exp[-e(\ln \alpha)L]. \tag{12}$$

Our work makes this relationship precise by determining the exponent to be $e = \frac{1}{2}$ or, equivalently, the coefficient to be $c_1 = \frac{1}{2} \ln \alpha$.

The $D^{-1/2}$ behavior is difficult to convincingly show from calculations for a fixed nonintegrable Hamiltonian. We have therefore used a control parameter to move away from an integrable Hamiltonian; this makes clear the trend of e approaching $\frac{1}{2}$ as one tunes away from integrability. In addition, the sizes at which the $D^{-1/2}$ behavior sets in are at the limit of sizes that can be comfortably addressed by full numerical diagonalization, which is the method used in current numerical studies of the ETH. Our use of sparse matrices with the shift-and-invert algorithm (see Appendix C 1) has allowed us to reach larger sizes: We have used full diagonalization for sizes up to $D \sim 2 \times 10^4$ and sparse-matrix methods for larger D, the largest being above 10^5.

While the exponent $e = \frac{1}{2}$ has not appeared for the EEV fluctuations in the setting of condensed-matter Hamiltonians, some similar or related results exist. The observations of Ref. [17] could be combined to construct an argument for $D^{-1/2}$ scaling, as discussed in Sec. IV C. In the literature on typicality [29–33], there is the expectation that the deviation of random Hamiltonians from typicality (closely related to the ETH) scales with system size such that measures of atypicality behave as $\sim D^{-1/2}$. Reference [30] shows this numerically for random Hamiltonians but finds other exponents for spin-chain Hamiltonians, for the sizes treated. Further work is needed for a full understanding of the connection between these results and ours.

Our work introduces several questions. First, the $D^{-1/2}$ behavior does not set in at smaller sizes. It is obvious from Figs. 3(d), 3(e), and 4 that larger sizes are necessary when integrability is weakly broken since the e values calculated from available sizes do not reach $\frac{1}{2}$ for λ near the integrable points. This indicates a length scale associated with the degree of integrability breaking, a concept that might be possible to explore quantitatively. Second, our quantitative result $\sigma_{\Delta A} \sim D^{-1/2}$ requires a finite Hilbert-space dimension D. It is not obvious how to generalize this law to continuum systems. Finally, it would be interesting to ask how the finite-size behavior of EEVs is affected by proximity to (many-body) localization, which, like integrability, is expected to be detrimental for thermalization.

ACKNOWLEDGMENTS

We thank P. Ribeiro, M. Rigol, and A. Sen for useful discussions.

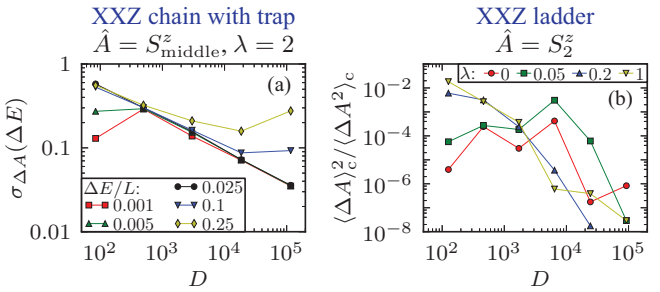

FIG. 6. (Color online) (a) Fluctuation amplitudes as a function of D for several widths ΔE of the microcanonical window. The value $\Delta E/L = 0.025$ (black curve) is used for the analysis in the rest of this work. The values 0.001 and 0.25 are extreme cases. (b) Average value $\langle \Delta A_\alpha \rangle^2_c$ divided by $\langle \Delta A^2_\alpha \rangle_c$ as a function of Hilbert-space dimension D for the ladder system with $\hat{A} = S^z_2$ for several values of λ. The lines connecting the points serve as a guide to the eye.

APPENDIX A: DEFINITION ISSUES FOR EEV FLUCTUATIONS

The width of the microcanonical window has been chosen to satisfy $\Delta E = 0.025L$, as a good compromise between the conditions that it contain sufficiently many eigenstates for good statistics and that the microcanonical average follows the EEVs well. To justify the choice of this value, we have plotted the fluctuation amplitudes $\sigma_{\Delta A}$ as a function of system size D for several values of ΔE in Fig. 6(a). Here we have chosen the observable $\hat{A} = S^z_{\rm middle}$ for the trap system at $\lambda = 2$, which is characterised by a strongly nonlinear dependence of the microcanonical average $\langle A \rangle_\mu(E, \Delta E)$ on E. This situation is a worst-case scenario: We expect a relatively strong dependence of the resulting $\sigma_{\Delta A}$ on ΔE because for very large values, the microcanonical average does not follow the actual EEVs $A_{\alpha\alpha}$ well. This mechanism is responsible for the fact that for very large values of ΔE, the fluctuations are overestimated [see Fig. 6(a)]. In the case where $\langle A \rangle_\mu(E, \Delta E)$ would depend almost linearly on ΔE, the dependence of $\sigma_{\Delta A}$ on ΔE will be weaker. Another feature that we find from Fig. 6(a) is that the fluctuations are underestimated if the number of states in the microcanonical average is very small in the case of small ΔE and small system size. Finally, we may conclude from Fig. 6(a) that $\sigma_{\Delta A}$ is almost independent of ΔE for a large range of values around $\Delta E/L = 0.025$. Here we emphasize that the values $\Delta E/L = 0.001$ and 0.25 present very extreme cases, where the microcanonical window encompasses only a few eigenstates (for the smaller system sizes) and almost the whole spectrum, respectively.

In order for the interpretation of $\sigma_{\Delta A}$, as defined by Eq. (2), as the standard deviation of the ΔA_α to be valid, we must test the condition that the average of ΔA_α is negligibly small, expressed by Eq. (4). In Fig. 6(b) we plot the ratio $\langle \Delta A_\alpha \rangle^2_c / \langle \Delta A^2_\alpha \rangle_c$ for the observable $\hat{A} = S^z_2$ in the ladder system as a function of the Hilbert space D and for several values of λ. We indeed observe that $\langle \Delta A_\alpha \rangle^2_c$ is negligibly small compared to $\langle \Delta A^2_\alpha \rangle_c$. The approximation $\mathrm{var}(\Delta A_\alpha) \equiv \langle \Delta A^2_\alpha \rangle_c - \langle \Delta A_\alpha \rangle^2_c \approx \langle \Delta A^2_\alpha \rangle_c$ generally improves for increasing system size. Thus, the interpretation of $\sigma_{\Delta A}$ as the standard deviation of the ΔA_α is justified.

APPENDIX B: MECHANISM FOR $D^{-1/2}$ DECAY OF EEV FLUCTUATIONS

In this section we expand on the argument provided in Sec. IV C for the $D^{-1/2}$ decay of EEV fluctuations. The $D^{-1/2}$ behavior arises from the fact that the individual eigenstates have D components and not from the sum over $O(D)$ different eigenstates in the definition of $\sigma_{\Delta A}$.

$D^{-1/2}$ from randomness of coefficients. Our argument is based on the expansion of the energy eigenstates $|\psi_\alpha\rangle$ in the basis of eigenvectors $|\phi_\gamma\rangle$ (with eigenvalues a_γ) of the operator $\hat{A}$, as given by Eq. (9). The EEVs are then realizations of a random variable that is the average of D approximately random variables,

$$A_{\alpha\alpha} = \sum_{\gamma=1}^{D} |c_\gamma^{(\alpha)}|^2 a_\gamma = \frac{1}{D} \sum_{\gamma=1}^{D} X_\gamma, \tag{B1}$$

where $X_\gamma = D|c_\gamma^{(\alpha)}|^2 a_\gamma$. We will now regard X_γ as random, quasi-independent, variables. There is no rigorous justification for this, but it can be argued in the same spirit as the arguments in favor of the ETH itself, namely, in a large nonintegrable system the typical eigenstate is so complicated that its components are effectively random in any reasonable basis. In principle, the randomness of $|c_\gamma^{(\alpha)}|^2$ and of X_γ may be different due to the multiplication with the eigenvalues a_γ. However, if these eigenvalues take only very few ($\ll D$) different values, then $|c_\gamma^{(\alpha)}|^2$ is random if and only X_γ is.

Assuming that the X_γ act as random variables, the central limit theorem implies that the EEVs have the standard deviation $\sqrt{\mathrm{var}(X_\gamma)/D}$. If the variance of X_γ is approximately D independent (as argued below), the $D^{-1/2}$ dependence of the fluctuations follows immediately.

We emphasize again that our reasoning is based on the assumption that the $|c_\gamma^{(\alpha)}|^2$ are random enough that the central limit theorem can be used. The extent or exact nature of this randomness is not understood in detail. At or near integrability, $\sigma_{\Delta A}$ no longer scales as $D^{-1/2}$, which suggests that the coefficients $|c_\gamma^{(\alpha)}|^2$ lose their randomness in such situations.

Even in the nonintegrable case, the assumption is invalid for any *conserved* quantity A. If $\hat{A}$ commutes with $\hat{H}$, one can choose a common eigenbasis and consequently only one $c_\gamma^{(\alpha)}$ is nonzero.

$\mathrm{var}(X_\gamma)$ *is independent of* D. We now argue that the variance of $X_\gamma = D|c_\gamma^{(\alpha)}|^2 a_\gamma$ is independent of D. The eigenvalues a_γ of the operator $\hat{A}$ are typically polynomial in system size and hence at most logarithmic in D. In addition, the average value of $|c_\gamma^{(\alpha)}|^2$ is $1/D$ by normalization. If the distribution of $|c_\gamma^{(\alpha)}|^2$ is not extremely pathological, this implies that the variance of $|c_\gamma^{(\alpha)}|^2$ scales as $1/D^2$. With this observation, it follows that $\mathrm{var}(X_\gamma) \sim 1$, i.e., constant in system size.

The variance of X_γ can be related to the PR through

$$P_\alpha/D = \left[1 + \mathrm{var}\left(D|c_\gamma^{(\alpha)}|^2\right)\right]^{-1} \sim [1 + \mathrm{var}(X_\gamma)]^{-1}, \tag{B2}$$

where the PR has been defined in Eq. (11). Thus, our previous statements are confirmed if the average scaled PR is constant as a function of system size. In addition to Fig. 5 we present a more detailed view of the PRs in Fig. 7. The average scaled

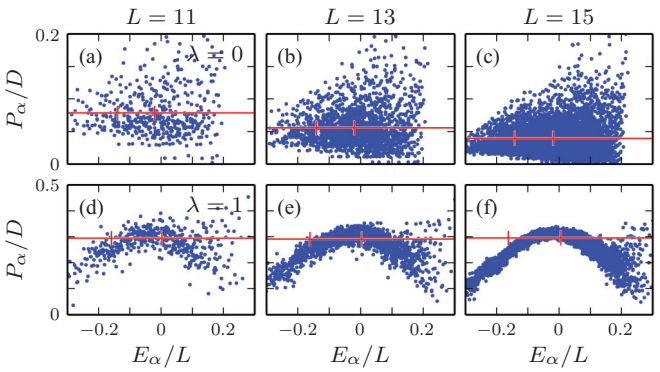

FIG. 7. (Color online) Scaled participation ratios P_α/D as a function of E_α in the Heisenberg XXZ ladder system. We show the results for system sizes $L = 11,13,15$ and two values of the control parameter: (a)–(c) $\lambda = 0$ and (d)–(f) $\lambda = 1$. The horizontal red line indicates the average scaled PR. The two vertical bars enclose the middle 20% of the spectrum, the energy region for which the average is taken. Here we have chosen the computational basis, which is also an eigenbasis for most of the observables discussed in the text (e.g., S_i^z, $S_i^z S_{i+1}^z$).

PR decreases noticeably with size in the integrable case, while it remains constant for nonintegrable systems.

Normal distribution of $A_{\alpha\alpha}$. The central limit theorem not only gives a value for the variance, it also states that the distribution of the $A_{\alpha\alpha}$ variables should be a normal distribution for large D. In support of this statement, we present the distributions of the fluctuations ΔA_α in Fig. 8. The distributions show the fluctuations within one window of the microcanonical average centered at $E/L = -0.1$, 0, and 0.1. The results closely resemble normal distributions, indicated by the dashed curves. This provides indirect support to the conjecture that the coefficients $|c_\gamma^{(\alpha)}|^2$ are effectively random.

APPENDIX C: COMPUTATIONAL DETAILS OF SPARSE-MATRIX METHODS AND HILBERT-SPACE SIZES

Hamiltonians in condensed matter physics generally lead to sparse matrices, so it is often advantageous to use sparse-matrix methods such as the Lanczos algorithm, which accesses the lowest or highest parts of the eigenspectra. In studies of the ETH, however, we explicitly want to access parts of the spectrum away from the edges. In addition, we have taken the approach of looking at the entire bulk of the spectrum. Therefore, as conventional in computational research on the ETH, we have used full diagonalization of the Hamiltonian matrix in order to treat Hilbert-space dimensions up to $D \approx 20\,000$. However, in this work, we have additionally gone beyond this size limit by using sparse-matrix methods that access nonextremal parts of the spectrum. This method is described in Appendix C 1. In Appendix C 2 we connect Hilbert-space sizes to system sizes for our three model systems.

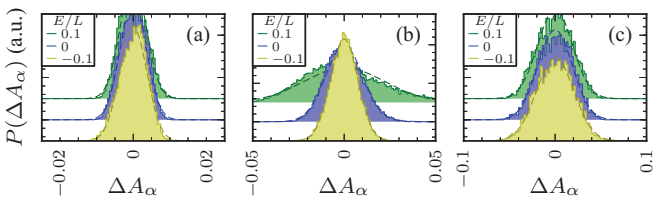

FIG. 8. (Color online) Histograms of the fluctuations ΔA_α in a microcanonical window. (a) Ladder system with $(L,N_\uparrow) = (19,9)$, $\hat{A} = C^z_{2,p+2}$, and $\lambda = 1$. (b) Magnetic-trap system with $(L,N_\uparrow) = (21,7)$, $\hat{A} = S^z_2$, and $\lambda = 2$. (c) Bose-Hubbard system with $(L,N_b) = (14,7)$, $\hat{A} = b_2^\dagger b_3 + b_3^\dagger b_2$, and $\lambda = 0.5$. For each system we show the distributions at the three energies defined by $E/L = -0.1,0,0.1$. The dashed curves indicate normal distributions with the same variances as those of the fluctuations ΔA_α.

1. Sparse-matrix methods

In order to tackle larger systems than can be comfortably accessed with full diagonalization on present-day machines, we have used a divide-and-conquer technique to split the problem of diagonalization into smaller parts. We used the so-called shift-invert algorithm: For a matrix H and a chosen value γ, one applies Lanczos diagonalization to the matrix $(H - \gamma I)^{-1}$ so that one effectively finds the eigenvalues of H close to γ. In practice, one does not invert the matrix explicitly since that would generate a nonsparse inverse matrix. Instead, the generation of the Krylov basis $\{\psi_i\}$, defined through $\psi_{i+1} = (H - \gamma I)^{-1}\psi_i$, is performed by iteratively solving $(H - \gamma I)\psi_{i+1} = \psi_i$. There is thus an inner iteration necessary for generating the Krylov basis in addition to the usual Lanczos iteration. Such methods are often known as inner-outer iterative methods.

While this method clearly takes significantly more run-time than bare Lanczos diagonalization, it has the advantage that any part of the spectrum can be accessed. For intermediate Hilbert-space sizes ($D \sim 10\,000$), we have performed several comparisons between the results of the sparse and the dense methods and we have found them to yield consistent results.

In order to find all eigenvalues and eigenstates of a large sparse matrix, we choose a set of initial energies $\{\gamma_i\}$ and compute in parallel typically 2000 eigenvalues close to each of these values together with the EEVs for a set of observables. Each application of the shift-invert method yields the eigenvalues within a certain (*a priori* unknown) energy interval. Afterwards, the results are patched together, i.e., for the energy regions where two or more such intervals overlap, the eigenvalues and EEVs are compared and duplicates are removed such that each appears only once in the final result. Finally, the total number of eigenvalues is compared against the known dimension of the Hilbert space. If the result does not contain all the eigenstates, more shift-invert diagonalizations are performed until all eigenstates have been obtained. The largest system for which we have found the full eigenspectrum using this procedure is of Hilbert-space dimension $D = 116\,280$.

2. Hilbert-space dimensions and system sizes

Our results on the EEV fluctuations have been presented in terms of the Hilbert-space dimension D. In order to translate the results to system size L, one uses the relations

$$D = \binom{L}{N_\uparrow}, \quad D = \binom{L + N_b - 1}{N_b} \tag{C1}$$

TABLE I. Overview of the system sizes L and Hilbert-space dimensions D of the models used. The cases with boldface values have been investigated with the sparse diagonalization algorithm; in all other cases, full diagonalization has been used. For the XXZ ladder model $u = 2$, $v = 1$, and $w = 1$; for the XXZ trap model $u = 3$, $v = 1$, and $w = 0$; and for the Bose-Hubbard model $u = 2$, $v = 1$, and $w = 0$.

			XXZ ladder model			
p	4	5	6	7	**8**	**9**
L	9	11	13	15	**17**	**19**
$N_\uparrow$	4	5	6	7	**8**	**9**
D	126	462	1716	6435	**24310**	**92378**
			XXZ trap model			
p	3	4	5	6	**7**	
L	9	12	15	18	**21**	
$N_\uparrow$	3	4	5	6	**7**	
D	84	495	3003	18564	**116280**	
			Bose-Hubbard model			
p	3	4	5	6	**7**	
L	6	8	10	12	**14**	
N_b	3	4	5	6	**7**	
D	56	330	2002	12376	**77520**	

for an L-site XXZ model with $N_\uparrow$ spins up and for an L-site Bose-Hubbard model with N_b bosons, respectively. In our numerical study, we approach the thermodynamic limit with systems with (almost) constant filling fraction $f \equiv v/u$ for integers u and v. We perform our calculations for the sequences $(L, N_\uparrow) = (up + w, vp)$ and $(L, N_\mathrm{b}) = (up + w, vp)$ $(p = 1, 2, \ldots)$ for the XXZ and Bose-Hubbard models, respectively; w is an additional constant integer. Table I provides an overview of the choices of the parameters and the resulting system and Hilbert-space sizes for the models discussed in this work.

With a constant filling fraction v/u, the Hilbert-space dimensions of Eq. (C1) can be approximated using Stirling's formula as

$$D \to \frac{\sqrt{c_{u,v}}}{\sqrt{2\pi p}} (\beta_{u,v})^p, \tag{C2}$$

where $c_{u,v}$ equals $u/v(u - v)$ for the XXZ models and $(u + v)/uv$ for the Bose-Hubbard model and

$$\beta_{u,v} \equiv \begin{cases} u^u/v^v(u - v)^{u-v} & (XXZ \text{ model}) \\ (u + v)^{u+v}/u^u v^v & (\text{Bose-Hubbard model}) \end{cases} \tag{C3}$$

defines the limiting ratio $\lim_{p\to\infty} D_{p+1}/D_p$ between the Hilbert-space dimensions of two subsequent realizations in the sequence of system sizes. In other words, the dimension of the Hilbert space is approximately exponential in the system size L as $D \sim L^{\beta_{u,v}}$. Assuming the power-law behavior $\sigma_{\Delta A} \propto D^{-e}$ of the EEV fluctuations (with $e = \frac{1}{2}$ for nonintegrable models), we find that this quantity scales exponentially in the system size as $\sigma_{\Delta A} \approx \text{const} \times (2\pi L)^{e/2} (\zeta_f)^{-eL}$, where

$$\zeta_f \equiv (\beta_{u,v})^{1/u} = \begin{cases} 1/f^f(1 - f)^{1-f} & (XXZ \text{ model}) \\ (1 + f)^{1+f}/f^f & (\text{Bose-Hubbard model}) \end{cases} \tag{C4}$$

in terms of the filling fraction f.

[1] J. M. Deutsch, Phys. Rev. A **43**, 2046 (1991).
[2] M. Srednicki, Phys. Rev. E **50**, 888 (1994).
[3] M. Rigol, V. Dunjko, and M. Olshanii, Nature (London) **452**, 854 (2008).
[4] A. Polkovnikov, K. Sengupta, A. Silva, and M. Vengalattore, Rev. Mod. Phys. **83**, 863 (2011).
[5] C. Kollath, G. Roux, G. Biroli, and A. M. Läuchli, J. Stat. Mech. (2010) P08011.
[6] G. Roux, Phys. Rev. A **81**, 053604 (2010).
[7] A. Motohashi, Phys. Rev. A **84**, 063631 (2011).
[8] T. N. Ikeda, Y. Watanabe, and M. Ueda, Phys. Rev. E **84**, 021130 (2011).
[9] S. Genway, A. F. Ho, and D. K. K. Lee, Phys. Rev. A **86**, 023609 (2012).
[10] M. Rigol and M. Srednicki, Phys. Rev. Lett. **108**, 110601 (2012).
[11] E. Khatami, M. Rigol, A. Relaño, and A. M. García-García, Phys. Rev. E **85**, 050102 (2012).
[12] G. P. Brandino, A. De Luca, R. M. Konik, and G. Mussardo, Phys. Rev. B **85**, 214435 (2012).
[13] M. Rigol, Phys. Rev. A **80**, 053607 (2009).
[14] M. Rigol, Phys. Rev. Lett. **103**, 100403 (2009).
[15] L. F. Santos and M. Rigol, Phys. Rev. E **82**, 031130 (2010).
[16] V. A. Yurovsky and M. Olshanii, Phys. Rev. Lett. **106**, 025303 (2011).
[17] C. Neuenhahn and F. Marquardt, Phys. Rev. E **85**, 060101 (2012).
[18] A. C. Cassidy, C. W. Clark, and M. Rigol, Phys. Rev. Lett. **106**, 140405 (2011).
[19] T. N. Ikeda, Y. Watanabe, and M. Ueda, Phys. Rev. E **87**, 012125 (2013).
[20] R. Steinigeweg, J. Herbrych, and P. Prelovšek, Phys. Rev. E **87**, 012118 (2013).
[21] E. Fradkin, *Field Theories of Condensed Matter Systems* (Perseus Books, New York, 1997); P. Kasteleijn, Physica **18**, 104 (1952); H. Bethe, Z. Phys. **71**, 205 (1931); M. Takahashi and M. Suzuki, Prog. Theor. Phys. **48**, 2187 (1972).
[22] T. Kinoshita, T. Wenger, and D. S. Weiss, Nature (London) **440**, 900 (2006).
[23] M. P. A. Fisher, P. B. Weichman, G. Grinstein, and D. S. Fisher, Phys. Rev. B **40**, 546 (1989); D. Jaksch, C. Bruder, J. I. Cirac, C. W. Gardiner, and P. Zoller, Phys. Rev. Lett. **81**, 3108 (1998); D. Jaksch and P. Zoller, Ann. Phys. (N.Y.) **315**, 52 (2005); M. Lewenstein, A. Sanpera, and V. Ahufinger, *Ultracold Atoms in Optical Lattices: Simulating Quantum Many-Body Systems* (Oxford University Press, Oxford, 2012).
[24] M. Rigol and M. Fitzpatrick, Phys. Rev. A **84**, 033640 (2011).
[25] K. He and M. Rigol, Phys. Rev. A **85**, 063609 (2012).
[26] C. Gramsch and M. Rigol, Phys. Rev. A **86**, 053615 (2012).

[27] M. Kollar, F. A. Wolf, and M. Eckstein, Phys. Rev. B **84**, 054304 (2011).
[28] K. He, L. F. Santos, T. M. Wright, and M. Rigol, Phys. Rev. A **87**, 063637 (2013).
[29] J. Gemmer, M. Michel, and G. Mahler, *Quantum Thermodynamics* (Springer, Berlin, 2009).
[30] S. Dubey, L. Silvestri, J. Finn, S. Vinjanampathy, and K. Jacobs, Phys. Rev. E **85**, 011141 (2012).
[31] J. Gemmer and M. Michel, Eur. Phys. J. B **53**, 517 (2006).
[32] P. Reimann, Phys. Rev. Lett. **99**, 160404 (2007).
[33] S. Goldstein, J. L. Lebowitz, R. Tumulka, and N. Zanghì, Phys. Rev. Lett. **96**, 050403 (2006).